Invariant Polarization Signatures for Recognition of Hydrometeors by Airborne Weather Radars

Anatoliy Popov[1](✉), Eduard Tserne[1], Valerii Volosyuk[1], Simeon Zhyla[1], Vladimir Pavlikov[1], Nikolay Ruzhentsev[1], Kostiantyn Dergachov[1], Olena Havrylenko[1], Oleksandr Shmatko[1], Yuliya Averyanova[2], Ivan Ostroumov[2], Nataliia Kuzmenko[2], Olga Sushchenko[2], Maksym Zaliskyi[2], Oleksandr Solomentsev[2], Borys Kuznetsov[3], and Tatyana Nikitina[4]

[1] National Aerospace University "Kharkiv Aviation Institute", Kharkiv, Ukraine
a.v.popov@khai.edu
[2] National Aviation University, Kyiv, Ukraine
[3] State Institution "Institute of Technical Problems of Magnetism of the National Academy of Sciences of Ukraine", Kharkiv, Ukraine
[4] Kharkiv National Automobile and Highway University, Kharkiv, Ukraine

Abstract. Hydrometeors, such as thunderclouds, hail, and snow, pose a threat to the safety of civil aviation flights. For their timely detection, airborne weather radars with dual polarization of radiation, two-channel reception of reflected signals, and signal processing by artificial intelligence methods are used, which makes it possible to distinguish signatures for the detection and recognition of dangerous hydrometeors for flights. The dependence of the characteristics of the reflected signal on a variety of microphysical and macrophysical parameters requires an expansion of the signature space to improve the reliability of detection. This article proposes invariant polarization signatures of hydrometeors, which are defined on the basis of the coherent decomposition of eigenvalues and eigenvectors of the polarization backscattering matrix. Based on the data of experimental studies, it is shown that the polarization parameters of the radar target's eigenbasis allow distinguishing the degree of ordering of hydrometeor particles (a characteristic feature of thunderstorm core in clouds) and the parameters of the invariant polarization transfer functions of hydrometeors make it possible to estimate the phase state of the hydrometeor, the presence of ice particles in it, hail, etc. even when the radar observes some mixture of hydrometeors of various types. The obtained results will improve the efficiency of the application of artificial intelligence methods in airborne meteorological radars.

Keywords: Weather Radar · Polarization Signature · Backscattering Matrix Decomposition

© The Author(s), under exclusive license to Springer Nature Switzerland AG 2023
O. Gervasi et al. (Eds.): ICCSA 2023, LNCS 13956, pp. 201–217, 2023.
https://doi.org/10.1007/978-3-031-36805-9_14

1 Introduction

Flight safety today still depends on weather conditions. Airborne weather radars installed on civil aircrafts mainly use dual polarization of signals [1] and let generally estimate the danger of weather conditions and avoid risk areas during flight [2], providing information to avionic-specific equipment, such as Electronic Flight Bag (EFB) [3]. At the same time, they do not always ensure timely detection of possible icing zones [4], thunderstorm cores [5], a lightning hazard [6], or a hail area [7]. Airborne weather radars are constantly being improved [8–10], they become multifunctional [11], and apply the most modern technologies [12]. The use of artificial intelligence methods [1] increases the probability of detecting dangerous hydrometeors [13], enhances the accuracy of estimation of their parameters [14], and improves weather predictions [15, 16]. However, methods for information extraction about hydrometeors from a radar signal remain traditional [17], mainly integral estimates are used, such as reflectivity (Z) and differential reflectivity (ZDR), differential phase (DP) [18], linear depolarization ratio (LDR) and eigenvalues [19]. This reduces the efficiency of using machine learning methods and neural networks [13, 14], and also does not solve the problem of separation of hydrometeors mixtures [20].

In this paper, we propose an approach to extraction of polarimetric information about hydrometeors, based on the coherent concept of polarimetry [21] and the theory of polarization transfer functions, which showed good results in the experiment in detecting ground objects by their electrical properties [22, 23], but have not been studied for hydrometeors.

2 Microphysical Parameters of Hydrometeors

The polarization of the reflected by hydrometeors signals essentially depends on the microphysical parameters. Hydrometeors that scatter an electromagnetic wave (EMW) in the radio range (fogs, clouds, and precipitation) are assemblies of condensed water particles suspended or falling in the atmosphere in various phase states [24]. Thunderclouds, which have areas of volumetric electric charges that cause drops to stick together in strong electrostatic fields, pose a particular danger to flights. The presence of a charge on drops in thunderclouds leads to their greater flattening compared to drops in clouds of other shapes [6].

Precipitation is usually understood as hydrometeors that are observed near the earth's surface. The main causes of precipitation are two mechanisms known as the processes of formation of warm and cold rain [5]. When warm rains are formed, the initial growth of droplets in clouds happens due to the condensation of water vapor, and the further transition from cloudy drops to raindrops is caused by the coagulation of small droplets. Droplets growth leads to enlargement in their fall velocity until the steady fall velocity reaches its maximum value (about 9 m/s). A further increase in size leads to spontaneous destruction of large unstable drops. The process of formation of cold rains is initiated by the absorption of water on ice crystals, which leads to their growth, causing the drop of large crystals below the level of the zero isotherm and their melting with the formation of hailstones and water drops [7].

The characteristics of the reflected radar signal are affected not only by macroparameters of the hydrometeor, such as type, height, and linear dimensions but also by microparameters characterizing the properties of hydrometeors in the local (specific) volume: concentration, distribution of particles by size, orientation, shape and phase state, permittivity, the particles fall velocity. Microphysical parameters determine the integral parameters: water content, precipitation intensity, radar reflectivity, etc. [24].

The particle distribution of hydrometeors by size determines the power of the reflected signal [25]. The smallest raindrops have a size of tens of micrometers, the maximum droplet size can reach 6–7 mm, the maximum size of hailstones can reach 60 mm, and powder particles is 10–12 mm, the maximum size of snowflakes is 15–20 mm, generally the diameters of snowflakes are in the range from 2 to 5.5 mm [26]. With the same intensity, thunderstorm rain contains larger droplets than a downpour and incessant rain.

To describe the distribution of hydrometeor particles by size, such analytical functions as the gamma function, exponential and logarithmically normal distributions, and power functions are most often used [27].

The shape of hydrometeor particles depends both on their phase state and size and differs from spherical. Liquid drops with a radius of more than 1 mm have the shape of an oblate spheroid with a flattened base [24]. Their shape is described by the ratio $m = b/a$ of the particle size in the symmetry plane b to its size along the symmetry axis a: $m > 1$ for oblate spheroids and $m < 1$ for prolate spheroids. For hail particles, the ratio of the minimum and maximum sizes m ranges from 0.3 to 1.0, with the most common values being 0.75…0.8 [27]. Unlike drops, the shape of hailstones is practically independent of size. The particles of ice pellets have a shape close to spheroidal or conical, and the ratio m varies between 0.5… 0.9 and, on average, increases with an increase of particles volume. The crystals observed in the upper part of the clouds at low temperatures are the most anisotropic in their shape. The sizes of lamellar crystals vary from 20 μm to 10 mm in diameter and from 10 to 90 μm in thickness. The sizes of columnar crystals range from 20 μm to 3 mm in length and from 10 to 40 μm in thickness.

The depolarization of the reflected radar signal depends on the orientation of the hydrometeor particles in space. Depending on the inclination of the particles to the plane of the irradiating electromagnetic wave, the effective scatterers' length changes along directions orthogonal to the polarized signal components. This causes depolarization of the incident field. The orientation of a particle is determined by the tilt angle β (the angle between the projection of the particle's symmetry axis onto the wavefront plane and the vertical) and the orientation angle γ (the angle between the particle's symmetry axis and the wavefront plane) (see Fig. 1).

The tilt angle β of raindrops does not depend on the internal properties of the drop, and it's a function of external impacts (wind speed, ascending and descending air currents). The distribution of drops over the tilt angles has a rather narrow maximum near the vertical direction, the width of which at the level of 0.5 is, on average, 10…20°, the mean value depends on the horizontal component of the wind speed. Correlation between the parameters of the tilt angle distribution and the drop sizes is not observed [24].

Hail particles have a much less ordering of orientations; their average orientation is commonly close to vertical or horizontal. Ice crystals are oriented, as a rule, randomly

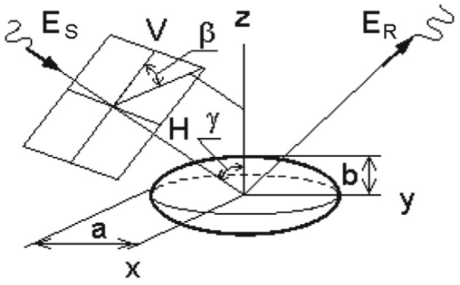

Fig. 1. Geometry of scattering on a hydrometeor particle.

in a horizontal plane. In the presence of a powerful electric field in thunderclouds, small crystals of all shapes tend to orient themselves with a high degree of an order along the direction of the electric field, which does not always coincide with the horizontal or vertical.

3 Radar Characteristics of Hydrometeors

A plane EMW falling on a single hydrometeor particle at an angle γ, excites a field inside it, which generates a scattered field. Let $\mathbf{E}_S$ be the electric field of the incident wave, $\vec{K}_1$ be a unit vector in the direction of incident wave propagation, and $\vec{K}_2$ be a unit vector directed from the coordinate origin to the observation point (see Fig. 1).

In the far field, the electric field of the scattered wave can be represented as

$$e_R(t) = \mathbf{E}_R \cdot \exp(j\omega \cdot t),\ \mathbf{E}_R = f\left(\vec{K}_1, \vec{K}_2\right) \cdot r^{-2} \cdot \exp(-j \cdot k \cdot r), \tag{1}$$

where $f\left(\vec{K}_1, \vec{K}_2\right)$ is the vector function specifying the scattering amplitude and the polarization of the scattered wave; r is the distance from the coordinate origin to the observation point; k is the EMW propagation constant in free space.

The amplitude of the incident wave in (1) is assumed to be a unit value. The scattering amplitude vector $f\left(\vec{K}_1, \vec{K}_2\right)$ is theoretically obtained from the solution of a boundary value problem on the surface of a hydrometeor particle [24].

It is known [17] that a complex polarization backscattering matrix (PBM) $\dot{\mathbf{S}}$ of size 2×2 gives a complete picture of the depolarizing properties of an object and relates the intensity of the emitted $\dot{\mathbf{E}}_S$ and the reflected from the object $\dot{\mathbf{E}}_R$ signals as

$$\dot{\mathbf{E}}_R = \dot{\mathbf{S}} \cdot \dot{\mathbf{E}}_S. \tag{2}$$

PBM describes the reflecting properties of an object at orthogonal polarizations at a given sensing frequency, and the squares of the modules of its elements correspond to the radar cross section (RCS) of the object

$$\sigma_{ij} = \left|\dot{S}_{ij}\right|^2 = \dot{S}_{ij}\dot{S}_{ij}^*.$$

Under the condition of propagation medium reciprocity, the PBM for the monostatic case is always symmetric [21]. In the "horizontal-vertical" {HV} polarization basis (PB), the PBM of a spheroidal particle with semi-axes a and b (see Fig. 1) can be written as:

$$\dot{\mathbf{S}} = \mathbf{Q}^{-1} \cdot \dot{\mathbf{S}}_0 \cdot \mathbf{Q}, \tag{3}$$

where $\mathbf{Q}$ is the unitary transformation matrix of the linear PB {HV} into the PB $\{\xi\eta\}$, associated with the projections of the ξ and η axes of the particle onto the plane of the wavefront

$$\mathbf{Q} = \begin{bmatrix} \cos\beta & \sin\beta \\ -\sin\beta & \cos\beta \end{bmatrix},$$

$\dot{\mathbf{S}}_0$ is the diagonal matrix whose elements $\dot{f}_\xi$, and $\dot{f}_\eta$ correspond to the reflection coefficients $f\left(\vec{K}_1, -\vec{K}_1\right)$ in (1) in the polarization basis $\{\xi\eta\}$.

PBM (3) can be rewritten as [24]:

$$\dot{\mathbf{S}} = \dot{\sigma}_0 \cdot \begin{bmatrix} 1 - \dot{\nu} \cdot \cos 2\beta & \dot{\nu} \cdot \sin 2\beta \\ \dot{\nu} \cdot \sin 2\beta & 1 + \dot{\nu} \cdot \cos 2\beta \end{bmatrix}, \tag{4}$$

where $\dot{\sigma}_0\big|_{\gamma=0} = \left(\dot{f}_\xi + \dot{f}_\eta\right)/2$ is the average amplitude of the reflected signal if $\gamma = 0^\circ$ (the axis of symmetry of the particle lies in the plane of the wavefront); $\dot{\nu}\big|_{\gamma=0} = \left(\dot{f}_\xi - \dot{f}_\eta\right)/\left(\dot{f}_\xi + \dot{f}_\eta\right)$ is the particle anisotropy coefficient.

Thus, the polarization backscattering matrix contains information about shape, orientation angles, and dielectric properties of reflecting particles.

The pulse volume of the radar contains N particles randomly located in space. The mean distance between the particles is much greater than the wavelength of the incident radiation and the mean particle size. Under such conditions, each particle of the assembly is an independent reflector, and the contribution of multiple scattering inside the volume can be considered negligible. Then the PBM of the considered volume of the hydrometeor can be written as the sum of N PBMs of all single independent reflectors that make up this volume [28]:

$$\dot{\mathbf{S}} = \sum_{i=1}^{N} e^{j\phi_i} \cdot \dot{\mathbf{S}}_i, \tag{5}$$

where ϕ is the random phase shift of signals reflected from different particles; it can take values from 0 to 2π with equal probability.

Taking into account the relative position of the radar and scattering particles, the signal from the impulse volume containing N hydrometeor particles is determined at the antenna input by the ratio:

$$\dot{\mathbf{E}}_\Sigma = \sum_{i=1}^{N} \frac{e^{jkR_i}}{jkR_i} \cdot \dot{\mathbf{S}}_i \dot{\mathbf{E}}_S,$$

where R_i is the distance from the i-nth particle to the antenna phase center; it is a random value that changes rapidly due to the particle motion. Therefore, the scattered field $\dot{\mathbf{E}}_\Sigma$ will also be a rapidly fluctuating random value.

When averaging over the range R within the radar pulse volume, which occurs in the radar receiver

$$\langle \dot{\mathbf{E}}_{\sum} \rangle_R = \sum_{i=1}^{N} \left\langle \frac{e^{jkR_i}}{jkR_i} \right\rangle \cdot \dot{\mathbf{S}}_i \dot{\mathbf{E}}_S,$$

at the output of the receiver we get a signal

$$\left| \langle E_{\sum} \rangle \right| \sim N \cdot |\langle S_i \rangle| \cdot \dot{\mathbf{E}}_S \tag{6}$$

proportional to the reflection coefficient from some mean hydrometeor particle, but this averaging takes place with account of the distribution of particles in size, orientation in space, shape, and other microphysical parameters.

Therefore, in radar meteorology, to study the shape, orientation, and phase state of hydrometeor particles and quantitative estimates of precipitation, a number of integral radar signatures are used.

Radar reflectivity (normalized RCS) for horizontally and vertically polarized waves Z_H and Z_V depends significantly on the type of hydrometeors, the concentration, and the size of particles in the pulse volume (large particles create the main power of the reflected signal [29]), and changes when particles pass from one phase state to other. The differential reflectivity $Z_{DR} = 10 \cdot \lg\left(Z_H \big/ Z_V\right)$ is used as a measure of the average ratio between the axes of the hydrometeor particles in the volume. One of the areas of practical use of Z_{DR} is the recognition of hail zones in powerful cumulus clouds [6].

The depolarization of the sensing signal is affected by the shape of the hydrometeor particles, the phase state, the permittivity, and the tilt angle with respect to the EMW polarization plane. To estimate the degree of EMW depolarization, linear depolarization ratios are used in H- and V-sensing [29]

$$LDR_H = 10 \cdot \lg\left(\left|\dot{S}_{HV}\right|^2 \Big/ \left|\dot{S}_{HH}\right|^2\right),\ LDR_V = 10 \cdot \lg\left(\left|\dot{S}_{VH}\right|^2 \Big/ \left|\dot{S}_{VV}\right|^2\right),$$

and a number of other radar parameters.

The discussed radar characteristics of hydrometeors are determined directly from the results of measurements of the polarization backscattering matrix (3) in the orthogonally linear polarization basis {HV} (the horizontal and vertical). They are used both for classifying hydrometeors and for their recognition by artificial intelligence methods as signatures, for example, in [1, 7, 13, 14].

4 Invariant Polarization Signatures of Radar Targets

The coherent approach [21] to the study of signals reflected by a radar target involves the use of full polarization information [30] obtained by modern radars [8, 9].

The complex amplitudes $\dot{E}_H$ and $\dot{E}_V$ of the orthogonally polarized components (6) form the polarization vector

$$\vec{\mathbf{E}} = \begin{bmatrix} E_H \cdot e^{j\psi_H} \\ E_V \cdot e^{j\psi_V} \end{bmatrix}. \tag{7}$$

While propagating, the electric field vector rotates with a periodically changing velocity, describing an ellipse in space. A complete revolution occurs during the period of the carrier frequency ω. The initial position of the vector $\vec{\mathbf{E}}$ inside the ellipse at the time $t = 0$ determines the phase of the elliptically polarized wave. The $\vec{\mathbf{E}}$ vector's direction of rotation is determined by the value of the phase difference $\delta = \psi_H - \psi_V$. For a quantitative description of an electromagnetic wave polarization, the geometric parameters of the polarization ellipse (Fig. 2) [21] are used. They are the ellipticity $\varphi\varphi$

$$\varphi = arctg\left(b/a\right), \varphi \in \left[-\frac{\pi}{4}, \frac{\pi}{4}\right], \tag{8}$$

where b and a are the minor and major semiaxes of an ellipse, and the orientation angle θ, that is the angle between the axis $\vec{n}_X$ and the major semi-axis of the ellipse; the orientation angle lies within the limits $\theta \in [0, \pi]$.

Signal parameters φ and θ can be determined out of the measurement results

$$tg(2\theta) = \frac{2|E_H| \cdot |E_V| \cdot \cos(\delta)}{|E_H|^2 - |E_V|^2}, \ \sin(2\varphi) = \frac{2|E_H| \cdot |E_V| \cdot \sin(\delta)}{|E_H|^2 + |E_V|^2}. \tag{9}$$

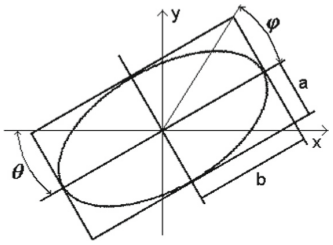

Fig. 2. Polarization ellipse parameters.

The measured polarization backscattering matrix $\dot{\mathbf{S}}$ (5) can be reduced to the diagonal form

$$\dot{\mathbf{S}}_E = \dot{\mathbf{Q}}^T_{\{\varphi_E, \theta_E\}} \cdot \dot{\mathbf{S}} \cdot \dot{\mathbf{Q}}_{\{\varphi_E, \theta_E\}}, \ \dot{\mathbf{S}}_E = \begin{bmatrix} \dot{\lambda}_1 & 0 \\ 0 & \dot{\lambda}_2 \end{bmatrix}, \tag{10}$$

where $\dot{\lambda}_1$, $\dot{\lambda}_2$ are eigenvalues; $\dot{\mathbf{Q}}_{\{\varphi_E, \theta_E\}}$ is the PBM eigenvectors (5).

In the polarimetry theory [21] eigenvectors are interpreted as polarizations of the object, which form the target's polarization eigenbasis $\ddot{\xi}_E = \{\varphi_E, \theta_E\}$, in which the signal reflection coefficients $\dot{\lambda}_1$ and $\dot{\lambda}_2$ will be maximum.

An approach alternative to (7) is the definition of an electromagnetic wave using a double complex plane [22, 23]

$$\ddot{E}(t) = E \cdot e^{-ij\varphi} e^{i\theta} e^{j\left(\omega t + \psi - 2\pi Z/\lambda\right)}, \tag{11}$$

where i is the spatial imaginary unit (the $(1, i)$ plane coincides with the electromagnetic wavefront plane); j is the temporal imaginary unit (direction of $(0, j)$ coincides with the

direction of electromagnetic wave propagation along the Z axis); E, ω, ψ and λ are the amplitude, frequency, phase, and wavelength; φ and θ are the angles of ellipticity (8) and orientation (9) of the electromagnetic wave.

When the signal $\ddot{E}_S$ is reflected by the target, the amplitude of the reflected signal $\ddot{E}_R$, its phase, and polarization changes, which in [22] is proposed to be represented in the formulation of the double complex plane in the form:

$$E_R \cdot e^{-ij\varphi_R} e^{i\theta_R} e^{j\psi_R} = \ddot{S}(\bullet) \times \left(E_S \cdot e^{-ij\varphi_S} e^{i\theta_S} e^{j\psi_S} \right), \tag{12}$$

where $\ddot{S}$ is the operator of transformation of the electromagnetic wave parameters that takes place when the wave is reflected from a target; $\times$ is the symbol for operator multiplication.

It is shown in [23] that the operator $\ddot{S}$ can be represented based on eigenvalues and eigenvectors $\dot{\vec{\lambda}}$ (10) of the polarization backscattering matrix of the target as a consecutive transformation of the amplitude $\Lambda(\dot{\vec{\lambda}})$, phase $e^{j\psi_T}$, orientation $\ddot{\Theta}(\theta_T)$, and ellipticity $\ddot{\Phi}(\varphi_T, \theta_E)$:

$$\ddot{S}\left(\vec{\lambda}, \ddot{\zeta}_E\right) = \Lambda(\dot{\vec{\lambda}}) \cdot e^{j\psi_T} \cdot \ddot{\Theta}(\theta_T) \cdot \ddot{\Phi}(\varphi_T, \theta_E), \tag{13}$$

where $\vec{\lambda} = \left[\dot{\lambda}_1, \dot{\lambda}_2\right]$ are the eigenvalues of the target's PBM; $\ddot{\zeta}_E = \zeta(\varphi_E, \theta_E)$ is the target's eigenpolarization (10); $\Lambda(\dot{\vec{\lambda}}) = \sqrt{\lambda_1^2 + \lambda_2^2}$ is the transfer function of the target in amplitude ($\lambda_1^2 + \lambda_2^2$ here means the maximum target's RCS); $e^{j\psi_T}$ is the signal phase transfer function; $\ddot{\Theta}(\theta_T) = e^{i\theta_T}$ is the transfer function of the orientation angle of the signal polarization vector; $\ddot{\Phi}(\varphi, \theta) = \left\{\ddot{\Theta}[-(\theta + \pi/4)] \times e^{-ij\varphi}\right\} \cdot \ddot{\Theta}(\theta + \pi/4)$ is the signal ellipticity transfer function; φ_T, θ_T and ψ_T are the transformations of the ellipticity, orientation, and phase of the signal parameters induced by the target. Parameters φ_T, θ_T and ψ_T are of interest in the problems of recognizing objects by their polarization properties since they depend only on the electrophysical and geometric characteristics of the reflecting object and do not depend on the type of sensing and received polarization, i.e. are invariant characteristics of the target.

In [31], a method for determining the parameters (13) was proposed. Based on the results of the target's polarization backscattering matrix (5) measurements with a four-channel full radar polarimeter in an orthogonal polarization basis, $\{H, V\}$ for example, the known relations can be used to find the eigenvalues $\dot{\vec{\lambda}} = \left[\dot{\lambda}_1, \dot{\lambda}_2\right]$ and eigenvectors $\dot{\mathbf{Q}}_{\{\varphi_E, \theta_E\}}$ PBM $\dot{\mathbf{S}}|_{HV}$.

Their ratio is calculated from the eigenvalues ($\dot{\lambda}_1 > \dot{\lambda}_2$):

$$\gamma_T = \arctan\left(\frac{|\lambda_2|}{|\lambda_1|}\right), \; \dot{p}_T = \frac{\dot{\lambda}_2}{\dot{\lambda}_1}, \; \Delta\psi_T = \arctan\left(\frac{\text{Im}\, \dot{p}_T}{\text{Re}\, \dot{p}_T}\right),$$

which are used to calculate the parameters of the operator (13):

$$\varphi_T = \tfrac{1}{2} \arcsin\{\sin(2\gamma_T) \cdot \sin(\Delta\psi_T)\}, \; \theta_T = \arctan\left\{\frac{\sin(2\gamma_T) \cdot \cos(\Delta\psi_T)}{\cos(2\gamma_T) + \cos(2\varphi_T)}\right\} \tag{14}$$

In this paper, we studied the possibility of using parameters (14) and parameters of the eigenbasis (10) φ_E, θ_E as signatures for recognizing the types of hydrometeors by polarimetric radar data.

5 Experimental Equipment

For the experimental research of reflections from hydrometeors, an experimental quadrature-polarimetric (Quad-Pol) X-band radar measuring system was used, built of standard airborne radars blocks with an improved antenna system. Our radar system operates in a pulse mode and contains one polarizing-isotropic reflector antenna (see Fig. 3) with an orthomode converter and an emitted pulses polarization switch, which allows emitting sensing pulses of vertical and horizontal polarization in turn. Reflected signals are received on the same reflector antenna. The orthomode converter separates the vertically polarized and horizontally polarized components of the reflected signal, which enter the two-channel receiver through the receive-transmit circulators. To expand the dynamic range of the receiver, the gain coefficients of the intermediate frequency amplifiers are digitally changing depending on the distance. High-speed analog-to-digital converters convert a fragment of an intermediate frequency signal specified by distance. This allows restoring the amplitude and phase of the received signals synchronously in two polarization-orthogonal channels. Thus, two successively emitted pulses with a time interval of 2.5 ms make it possible to measure the full polarization backscattering matrix. The radar has a built-in system for calibrating receivers with microwave pulses, which allows controlling the receiving channels' parameters during measurements. To improve the accuracy of measurements, an external active-passive calibration system is also used, which allows taking into account the errors of the transmitter, antenna, and non-identity of the receiving channels.

Main specifications of the Quad-Pol radar measuring system:

- transmitter power (in pulse) is 1 kW;
- working frequency is 9,37 GHz;
- pulse duration is 0,5 μs;
- receiver sensitivity is not less than 120 dB/mW;
- pulse repetition rate is 400 Hz;
- range of change of the emitted signal orientation angle is 0° to 90°;
- polarization modulator limit frequency is 10 kHz;
- antenna beamwidth (by zeros) is 3°;
- antenna cross-polarization level is not worse than 36 dB;
- polarizing separator decoupling degree is not worse than 38 dB;
- polarization basis setting error is not more than 0,1°.

During the experiments, the radar was installed on the roof of a high-rise building. The antenna position control system provided space scanning within the 270° in azimuth and 0…45° in elevation. Measurements of the polarization characteristics of hydrometeors were made at distances from 1 to 20 km in a movable window d = 2 km (see Fig. 3) with a fixed antenna to eliminate the effects of additional signal modulation due to antenna movement. Meteorological conditions were recorded according to the airport weather service.

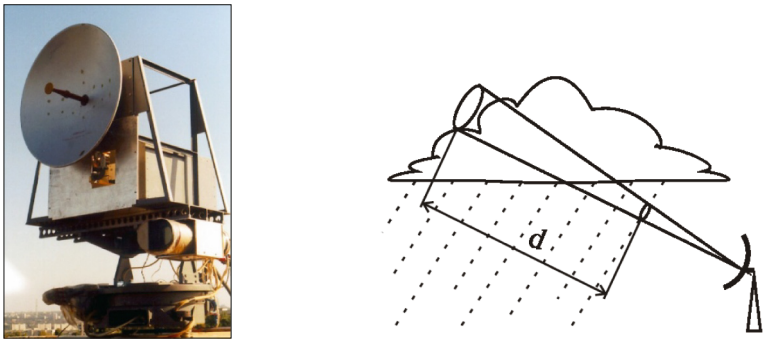

a) b)

Fig. 3. Quad-Pol radar (a) and experiment geometry (b).

6 Experimental Results

From the database obtained in field experiments the records of reflected by hydrometeors signals with approximately the same normalized RCS were selected for analysis, which complicates hydrometeors recognition task by energy characteristics.

Experimental studies of reflected by hydrometeors of various types (rain, hail, snow, thunderclouds, etc.) signals have shown that it is rather difficult to isolate a specific type of hydrometeor in a "pure" form during measurements. Figure 4 shows a radar image fragment of rain with an intensity of up to 10 mm/h when sensing with an elevation angle of 7.5°. At a distance of up to 1.5 km, the reflected signal is mainly formed by raindrops, over 2 km - mainly by a rain cloud. Figure 5 shows a radar rain image with a hail band (the size of ice particles, according to ground control data, reached 5 mm) at a distance of 1.5 km to 2.5 km. At short distances (up to 1.3 km), the reflected signal is formed by water particles in the liquid state. Therefore, mixes of hydrometeors of different types are present in almost any real data, which, as noted in [20], creates the problem of detecting dangerous for flight hydrometeors.

The RCS of hydrometeors fluctuates over a wide range (up to 60 dB), and the amplitude histograms of the reflected by different hydrometeors signals overlap. For example, Fig. 6 shows the experimentally obtained PBM S_{HH} and S_{HV} elements histograms of four hydrometeors (rain, hail, snow, thunderclouds). That means that it is rather difficult to determine the type of hydrometeors according to such traditional in radar meteorology signal parameters as reflectivity at different polarizations (Z_H, Z_V) when the hydrometeors intensities or water contents are close values.

The wide-range fluctuations of amplitudes of signals in polarization-orthogonal channels of the radar receiver are caused by fluctuation of polarization of the reflected signals.

Changes in signal polarization can be clearly seen in a polarimetric diagram [32] (Fig. 7), where each possible value of the ellipticity and orientation corresponds to a point in polar coordinates. Plotting of two-dimensional histograms of signals' ellipticity and orientation in the polarimetric diagram allows us to "see" the most probable signal polarization values areas. For example, Fig. 7-b shows histograms of the ellipticity and

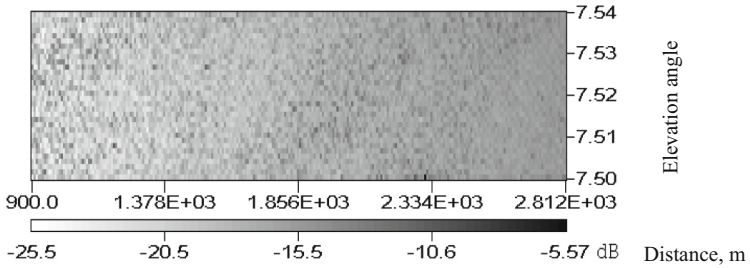

Fig. 4. Radar rain image, PBM element S_{VV}.

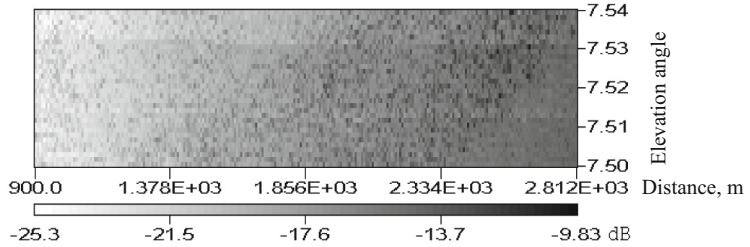

Fig. 5. Radar hail image, PBM element S_{VV}.

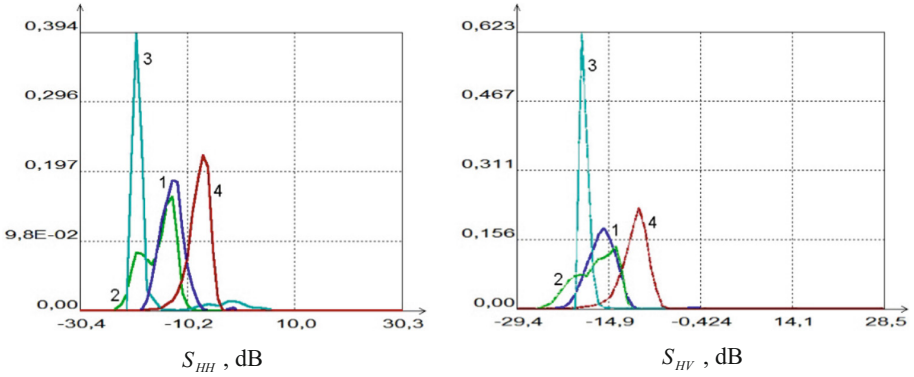

Fig. 6. Histograms of PBM elements S_{HH} (a), S_{HV} (b) of four types of hydrometeors (1 is a rain, 2 is a hail, 3 is a snow, 4 is a thunderclouds).

orientation of the signals reflected by rain and hail when they are sensed by a horizontally polarized signal. Figure 7 shows that backscattering changes both the ellipticity of the signal and its orientation. Moreover, the angle of the backscattered signal orientation rotation can reach 45°.

As orientation angles of hydrometeor particles are random, the projections of the reflected electric field vector according to (3) will have significant fluctuations, which

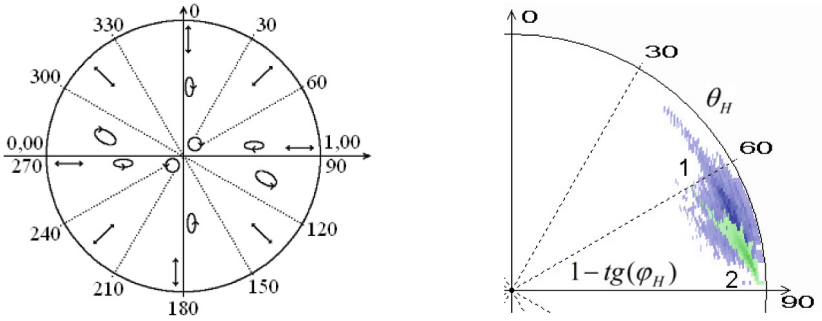

Fig. 7. Polarimetric diagram (a) and the histograms of polarization of the signals backscattered by rain (1) and hail (2) in the polarimetric diagram (b).

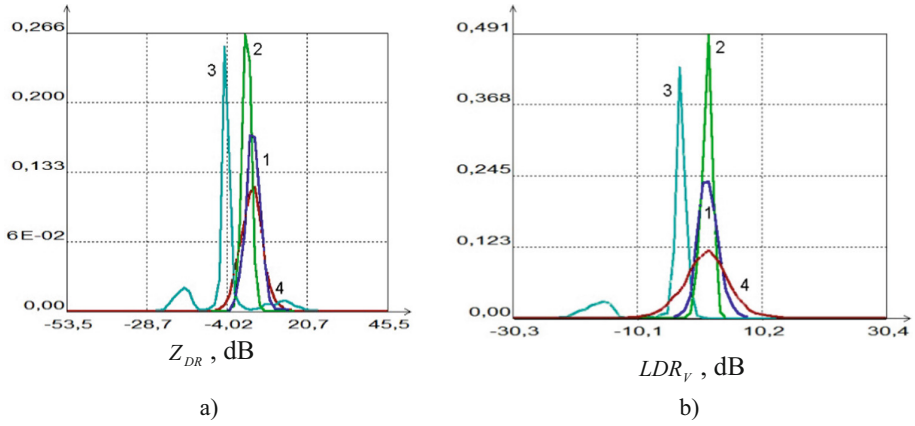

Fig. 8. Histograms of differential reflectivity (a) and linear depolarization ratio (b) for various types of hydrometeors: rain (1), hail (2), snow (3), thunderstorm (4).

is observed in the histograms of traditional relative radar characteristics, namely differential reflectivity Z_{DR} and linear depolarization ratios *LDR*. An example of these radar characteristics histograms is shown in Fig. 8.

A feature of the invariant polarization signatures discussed in Sect. 4 is that these signatures separate the sources of fluctuations in the reflected signal parameters. The parameters of the target's polarization eigenbasis φ_E, θ_E (eigenvectors (10)) show the changes in the signal associated with the target's orientation relative to the radar, and the parameters of polarization transformation by the target φ_T and θ_T describe the changes in the polarization of the signal backscattered by the target oriented in the radar coordinate system. Therefore, invariant polarization signatures have lower dispersion and are more compactly located in the polarimetric diagram.

Figure 9 shows the histograms of the polarization eigenbasis parameters plotted in the polarimetric diagram for the four studied types of hydrometeors. Analysis of the polarimetric diagrams shows that depending on the hydrometeor type the position of the

distribution mode for the object's eigenpolarizations shifts. If for the thunderclouds the mode of the eigenorientation θ_E is located near the orientation angle of 100°, for the rain of medium intensity it is about 110°, then for solid-phase hydrometeors it noticeably shifts towards larger angles: for hail it is approximately 130°, for dry snow it is almost 145°. With a relatively small dispersion of θ_E these objects become distinguishable.

The obtained result is quite understandable from the point of view of the microphysics of hydrometeors (see Sect. 2). There is a belief that in thunderclouds the water droplets are more flattened and more orderly oriented due to the presence of electrostatic electricity, which leads to a more pronounced "mean orientation" of the observed average droplet (6). Hail particles have much less orientation order, while snowflakes and ice crystals are oriented, as a rule, chaotically. So the signature θ_E can be used as an indicator for the degree of particles ordering in a hydrometeor.

The polarization transformation parameters φ_T and θ_T (14) turned out to be interesting for practical use. Studies [22, 23] have shown that they are sensitive to the target's electrophysical properties – dielectric permittivity and conductivity. Calculation of these parameters for hydrometeors showed that the polarization transformation parameters φ_T and θ_T clearly/strictly distinguish the phase state of the hydrometeor and group these objects into the classes "liquid water" and "solid" state (snow, ice).

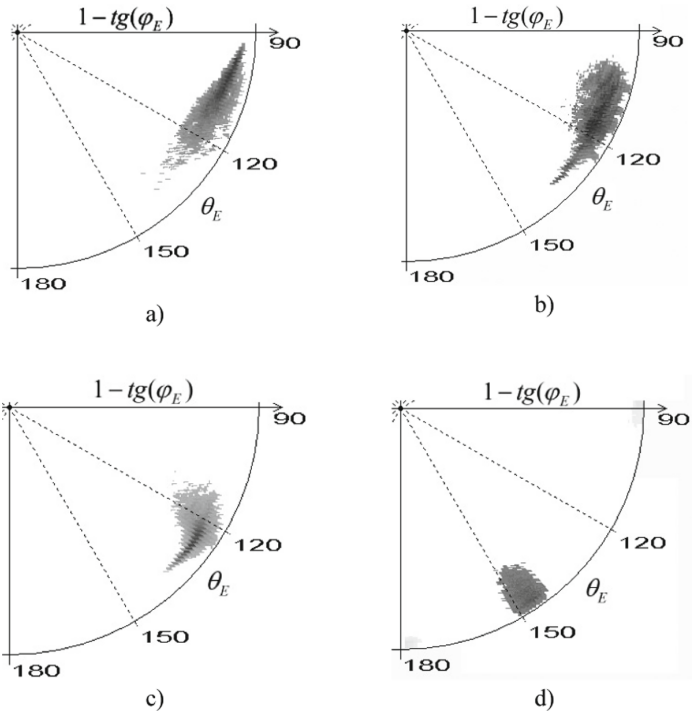

Fig. 9. Location of two-dimensional histograms of eigenellipticity φ_E and eigenorientation θ_E in the polarimetric diagram for various types of hydrometeors: storm (a), rain (b), hail (c), snow (d).

Figure 10 shows location of the polarization transformation φ_T and θ_T histograms of rain, thunderclouds (almost identical to rain), snow, and hail in the polarimetric diagram. To build the polarization transformation φ_T and θ_T histograms of hail we used the sample, which was shown in Fig. 5. Approximately half of the sample contain readouts of signals reflected from the hydrometeor in the liquid phase, therefore, in Fig. 10, the histogram of the "hail" object has a pronounced bimodal nature; part of the samples refers to the hydrometeor in the liquid state and it is almost identical to the rain in its position in the polarimetric diagram, and the second mode is shifted noticeably closer to the area occupied by snow. Thus, the polarization transformation parameters φ_T and θ_T can be used as indicators of the hydrometeor phase state.

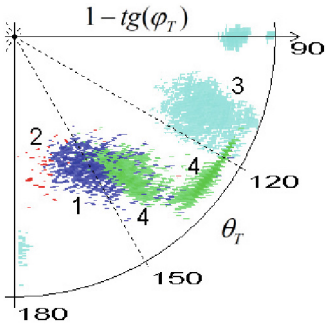

Fig. 10. Location of two-dimensional histograms of polarization transformation φ_T and θ_T of rain (1), thundercloud (2), snow (3), and hail (4) in the polarimetric diagram.

7 Conclusion

Bad weather conditions can lead to flight accidents and/or delays in civil aviation flights [33]. Modern weather radars installed on civil aviation aircrafts use dual polarization of sensing and two-channel reception of reflected signals. This makes it possible to measure the full polarization backscattering matrix and define signatures for detection and recognition of hydrometeors dangerous for flights.

Hydrometeors are complex non-stationary radar targets that may contain a mixture of different types of hydrometeors. The characteristics of the reflected signal depend on a variety of microphysical and macrophysical parameters. The signatures traditionally used to classify hydrometeors do not always provide timely and reliable danger detection. The use of modern artificial intelligence methods increases the probability of correct hydrometeors classification, but their effectiveness depends on the informativity of the initial data.

In this work we studied the informativity of hydrometeors invariant polarization signatures, which were derived on the basis of coherent decomposition of the polarization backscattering matrix, extracting its eigenvalues and eigenvectors, followed by the detailed treatment of decomposition results. This allowed us to identify new signatures that provide additional information about hydrometeors.

On the basis of our own experimental data we have shown that invariant polarization signatures based on the decomposition of the eigenvalues and eigenvectors of the polarization backscattering matrix make it possible to get the hydrometeor particles' degree of order, which is a characteristic feature of thunderstorm cores in clouds, and the phase state of the hydrometeor, the presence of ice particles in it, hail particles, etc.

No doubt, the obtained results are preliminary and require subsequent large-scale experimental studies. But the already available data suggest that expansion of the signature space for the artificial intelligence methods will increase the reliability of detecting hydrometeors dangerous for flights and, accordingly, will enhance the safety of civil aviation flights.

References

1. Chandrasekar, V.: AI in weather radars. In: 2020 IEEE Radar Conference (RadarConf20), pp. 1–3. IEEE, Florence, Italy (2020)
2. Cuccoli, F., Lupidi, A., Facheris, L., Baldini, L.: Polarimetric radar for civil aircrafts to support pilots' decision in bad weather conditions. In: 2015 IEEE International Geoscience and Remote Sensing Symposium (IGARSS), pp. 2327–2330. IEEE, Milan, Italy (2015)
3. D'Amico, M., et al.: The X-WALD project: towards a cleaner sky. In: 2014 44th European Microwave Conference, pp. 1888–1891. IEEE, Rome, Italy (2014)
4. Shrestha, Y., Zhang, Y., Fusselman, J., McFarquhar, G.M., Blake, W., Harrah, S.D.: Potential application of PARADOX (Polarimetric Airborne Radar Operating at X-band) to High Ice Water Content (HIWC) monitoring. In: 2022 IEEE Radar Conference (RadarConf22), pp. 1–6. IEEE, New York City, NY, USA (2022)
5. Nagel, D.: Detection of rain areas with airborne radar. In: 2017 18th International Radar Symposium (IRS), pp. 1–7. IEEE, Prague, Czech Republic (2017)
6. Wu, S., Si, J., Hu, D., Guo, Z., Zhang, Y., Zhao, Q.: Analysis of echo characteristics of dual-polarization Doppler weather radar in lightning weather. In: 2019 International Conference on Meteorology Observations (ICMO), pp. 1–4. IEEE, Chengdu, China (2019)
7. Schmidt, M., Trömel, S., Ryzhkov, A.V., Simmer, C.: Severe hail detection: hydrometeor classification for Polarimetric C-band radars using fuzzy-logic and T-matrix scattering simulations. In: 2018 19th International Radar Symposium (IRS), pp. 1–7. IEEE, Bonn, Germany (2018)
8. Yeary, M., Cheong, B.L., Kurdzo, J.M., Yu, T.-Y., Palmer, R.: A brief overview of weather radar technologies and instrumentation. IEEE Instrum. Meas. Mag. **17**(5), 10–15 (2014)
9. Berizzi, F., et al.: The X-WALD project: first measurements in Europe with an avionic polarimetric weather radar. In: 2017 IEEE Radar Conference (RadarConf), pp. 0487–0491. IEEE, Seattle, WA, USA (2017)
10. Ren, Z., Wu, D., Gao, M., Shen, M., Zhu, D.: Clutter suppression for airborne weather radar using 3D-STAP. In: 2020 IEEE 5th International Conference on Signal and Image Processing (ICSIP), pp. 468–473. IEEE, Nanjing, China (2020)
11. Kunstmann, F., Klarer, D., Puchinger A., Beer, S.: Weather detection with an AESA-based airborne sense and avoid radar. In: 2020 IEEE Radar Conference (RadarConf20), pp. 1–6. IEEE, Florence, Italy (2020)
12. Vivekanandan, J., Karboski, A., Loew, E.: Airborne Polarimetric doppler weather radar: antenna aperture and beam forming architecture. In: 2019 IEEE International Symposium on Phased Array System & Technology (PAST), pp. 1–6. IEEE, Waltham, MA, USA (2019)

13. Yu, Q., Wu, D., Zhu, D., Qian, J.: CNN-based weather signal detection algorithm for airborne weather radar. In: 2020 IEEE 5th International Conference on Signal and Image Processing (ICSIP), pp. 660–664. IEEE, Nanjing, China (2020)
14. Wang, L., Chen, H.: Machine learning for polarimetric radar quantitative precipitation estimation. In: 2023 United States National Committee of URSI National Radio Science Meeting (USNC-URSI NRSM), pp. 298–299. IEEE, Boulder, CO, USA (2023)
15. Zhang, J., Chen, H., Han, L.: An investigation of a probabilistic nowcast system for dual-polarization radar applications. In: IGARSS 2020 - 2020 IEEE International Geoscience and Remote Sensing Symposium, pp. 5294–5297. IEEE, Waikoloa, HI, USA (2020)
16. Yao, S, Chen, H., Thompson, E.J., Cifelli, R.: An improved deep learning model for high-impact weather Nowcasting. IEEE J. Sel. Top. Appl. Earth Obs. Remote Sens. **15**, 7400–7413 (2022)
17. Yanovsky, F.: Retrieving information about remote objects from received signals. In: 2022 IEEE 2nd Ukrainian Microwave Week (UkrMW), pp. 512–517. IEEE, Kharkiv, Ukraine (2022)
18. Biswas, S.K., Cifelli, R., Chandrasekar, V.: Quantitative precipitation estimation using X-band radar for orographic rainfall in the San Francisco bay area. IEEE Trans. Geosci. Remote Sens., 1 (2022)
19. Galletti, M., Gekat, F., Goelz, P., Zrnic, D.S.: Eigenvalue signal processing for phased-array weather radar polarimetry: removing the bias induced by antenna coherent cross-channel coupling. In: 2013 IEEE International Symposium on Phased Array Systems and Technology, pp. 502–509. IEEE, Waltham, MA, USA (2013)
20. Pejcic, V., Simmer, C., Trömel, S.: Polarimetric radar-based methods for evaluation of hydrometeor mixtures in numerical weather prediction models. In: 2021 21st International Radar Symposium (IRS), pp. 1–10. IEEE, Berlin, Germany (2021)
21. Boerner, W.-M., Yan, W.-L., Xi, A.-Q., Yamaguchi, Y.: On the basic principles of radar polarimetry: the target characteristic polarization state theory of Kennaugh, Huynen's polarization fork concept, and its extension to the partially polarized case. Proc. IEEE **79**(10), 1538–1550 (1991)
22. Popov, A., Bortsova, M.: Detection of metal objects against mountain ranges using polarization transfer functions. In: 2018 IEEE 17th International Conference on Mathematical Methods in Electromagnetic Theory (MMET), pp. 290–293. IEEE, Kyiv, Ukraine (2018)
23. Popov, A., Bortsova, M.: Experimental research of polarization transfer functions of mobile ground objects. In: 2019 IEEE 2nd Ukraine Conference on Electrical and Computer Engineering (UKRCON), pp. 119–122. IEEE, Lviv, Ukraine (2019)
24. Oguchi, T.: Electromagnetic wave propagation and scattering in rain and other hydrometeors. Proc. IEEE **71**(9), 1029–1078 (1983)
25. Zrnic, D., Ryzhkov, A., Fulton, R.: Classification and measurement of precipitation using a dual-polarization radar. In: IEEE 1999 International Geoscience and Remote Sensing Symposium. IGARSS 1999, pp. 711–713. IEEE, Hamburg, Germany (1999)
26. El-Magd, A., Chandrasekar, V., Bringi, V.N., Strapp, W.: Multiparameter radar and in situ aircraft observation of graupel and hail. IEEE Trans. Geosci. Remote Sens. **38**(1), 570–578 (2000)
27. Straka, J.M., Zrnić, D.S., Ryzhkov, A.V.: Bulk hydrometeor classification and quantification using polarimetric radar data: synthesis of relations. J. Appl. Meteorol. Climatol. **39**, 1341–1372 (2000)
28. Mishchenko, M.I.: Electromagnetic scattering by nonspherical particles: a tutorial review. J. Quant. Spectrosc. Radiat. Transfer **110**(11), 808–832 (2009)
29. Wolf, D.A., Russchenberg, W.J., Ligthart, L.P.: Radar reflection from clouds: gigahertz backscatter cross sections and Doppler spectra. IEEE Trans. Antennas Propag. **48**(2), 254–259 (2000)

30. Chen, S.: Polarimetric coherence pattern: a visualization and characterization tool for PolSAR data investigation. IEEE Trans. Geosci. Remote Sens. **56**(1), 286–297 (2018)
31. Popov, A., Bortsova, M.: Polarization transfer functions of remote sensing objects. In: 9th International Kharkiv Symposium on Physics and Engineering of Microwaves, Millimeter and Submillimeter Waves (MSMW 2016), pp. 1–4. IEEE, Kharkiv, Ukraine (2016)
32. Popov, A.V., Pogrebnyak, O.: Informativity of polarimetric radar invariants. In: SPIE's 48th Annual Meeting on Optical Science and Technology, Earth Observing Systems VIII, vol. 5151, pp. 74–84. San Diego, California, United States (2003)
33. Ostroumov, I., et al.: A probability estimation of aircraft departures and arrivals delays. In: Gervasi, O., et al. (eds.) ICCSA 2021. LNCS, vol. 12950, pp. 363–377. Springer, Cham (2021). https://doi.org/10.1007/978-3-030-86960-1_26